Numerical Simulation of Two-Phase Slug Flow Liquid-Carryover in a Converging T-junction

Minh Cong Tran, Hai Anh Nguyen, and Dat Tien Nguyen

***Abstract*—In the offshore platform, T-junction has been extensively used as preliminary gas-liquid separator due to its compact design. Frequently, a sudden slug generation causes liquid carryover issues leading to excessive liquid in the gas feed for downstream equipment. Geometry features of T-junction and slug flow are believed to be the root cause of this problem. Based on the literature review, previous works mostly focused on improving two-phase separation in the standard T-junctions without taking into account the impact of inlet flow regime. Moreover, there is no published research on the separation performance of converging T-junction, which is a promising design. The objective of this research is to numerically evaluate the hypothesis that converging T-junction yields better phase separation under slug flow compared with regular and reduced T-junctions. Three-dimensional Computational Fluid Dynamics (CFD) software FLUENT 17.2 and specialized User Defined Functions was utilized to study the evolutionary process of air-water slug flow and its phase separation behavior in converging T-junctions over eight different geometry designs. The incompressible Volume of Fluid (VOF) method was used to capture the transient distribution of segregated gas-liquid interface. The validity of the present model was compared with the experimental data taken from the air-water two-phase flow in 3-inch diameter main pipe of T-junction. The validated model gave a strong foundation to proceed with converging T-junction simulation. The research found that the converging T-junction can increase by upto 20% of separation efficiency compared with regular and reduced T-junction at the same operating conditions. Moreover, the converging T-junction with the main and converging diameter ratio of 0.67 and 0.4, respectively, to be optimal in improving the phase separation over a wide spectrum of air and water superficial velocities.**

***Index Terms*—Numerical simulation, slug flow, T-junction, two-phase separation.**

I. Introduction

Excessive liquid carryover in gas feed stream extracted from the branch of T-junction causes severe issues for downstream equipment (Fig. 1). This causes the gas separation system to trip frequently for maintenance activities, which in fact, often takes at least two days to resume to normal operation. In the case of wells using artificial gas lifts, the trip time can be up to two weeks. Therefore, improving phase separation efficiency at a T-junction by reducing liquid carryover is crucial to solving this problem [1]. The current design of T-junction has not considered the effect of its geometry in all aspects as well as inlet flow regime on its separation split. In-depth literature survey reveals that the flow regime is one of the most dominant factors in multiphase flow research. Notably, some flow regimes, for example, slug flow, shows very complex behavior which intensifies the liquid carryover phenomenon [2], [3]. Therefore, it is necessary to investigate the behavior of the slug flow in the different geometrical design of T-junctions to improve the phase separation.

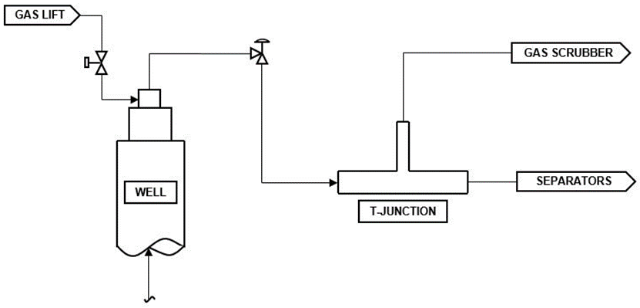

Fig. 1. Simplified schematic of multiphase flow from well to separation system.

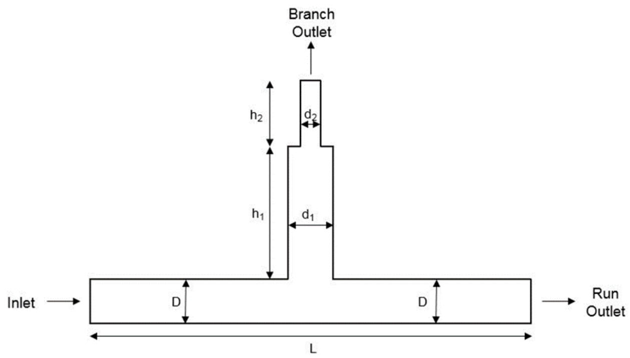

Fig. 2. Geometrical features in a converging combined T-junction.

Of all geometrical aspects, the diameter ratio between the branch arm and main arm is one of the most important factors to reduce liquid carryover. Many research works have been carried out to determine the optimal diameter ratio which delivers the lowest peak liquid carryover and highest liquid carryover threshold [1]. Most of them agreed that a reduction in diameter ratio could decrease peak liquid carryover, thus improve phase separation [4]-[9]. Recently, Saieed [9] proved that reducing the diameter ratio to a certain limit can decrease the liquid carryover threshold as well, thus worsen phase separation. Therefore, this work proposes a new design called the converging T-junction, which is expected to combine low peak liquid carryover and high liquid carryover threshold. Fig. 2 shows geometrical

Manuscript received September 3, 2019; revised January 11, 2020. This research was supported by Viettel High Technologies Corporation, Viettel Group in the research program of Modeling & Simulation Center and Control & Dynamic Department.

The authors are with the Modeling and Simulation Center – Viettel High Technologies Corporation, Vietnam (Corresponding author: Minh Cong Tran, minhtc3@viettel.com.vn).

doi: 10.18178/ijmmm.2020.8.3.490

parameters in a converging T-junction with branching type. It consists of the horizontal main pipe and the vertical branch arm including two parts with different diameters ($d_1 > d_2$). The ratio between d_1 and D is defined as the main diameter ratio (DR_1), while that between d_2 and D is considered as converging diameter ratio (DR_2). Thus, the proposed hypothesis is: compared with T-junctions having reduced diameter ratio, the converging T-junction can improve phase separation efficiency under slug flow condition.

Among many methods in CFD, Volume of Fraction (VOF) is used as a preference in studying intermittent flow in straight pipes. Cook *et al*. [10], Lorstard *et al*. [11] and Zhou [12] applied the VOF method to investigate 3D bubbles, which validated reasonably with experimental results. In case of slug flow, Taha *et al.* [13], Ujang *et al.* [14] and Febres [15] successfully simulate slug flow using VOF method, by generating bubbles moving along reference frame of slug flow in a pipeline.

In term of intermittent flow in T-junction, by tracking the interfaces, this paper uses VOF to study slug flow in T-junction to test stated hypothesis. The model was verified and validated with experimental data to affirm its authenticity and robustness to describe air-water two-phase slug flow in a T-junction and its behavior of separation at the intersection.

II. Methodology

A numerical method is required to solve a very complicated set of differential equations derived in the previous section. Overall, the procedure includes the steps as shown in Fig. 3.

- The geometry domain is subdivided into finite volumes.
- The partial differential equations are integrated over the finite volume and over time to yield to a set of non-linear algebraic equations. The boundary conditions are also put into an algebraic form.
- The system of equations can be solved numerically by replacing the partial derivatives by finite differences on a discrete numerical grid and then advancing the solution in time via some numerical schemes algorithm. The process is repeated until steady-state or the desired time level is reached.

A. Geometry Domain and Meshing

Geometry domain of T-junction was taken from air-water flow loop in Saieed's experiment [9]. Modeling geometry used in present model included the mixer and T-junction. A three-dimensional model of T-junction can be divided into main, run and branch arms (Fig. 4).

While the length of all arms and the main pipe diameter are fixed, different geometry designs of converging T-junction are characterized by different combinations of main and converging diameter ratios. Table I presents the combination of these diameter ratio making the different testing case in this study. It is noted that when main diameter ratio, DR_1, is equal to the converging diameter ratio, DR_2, the converging T-junction is considered as regular T-junction (DR 1.0-1.0 design) or reduced T-junction (DR 0.67-0.67 design).

B. Boundary Conditions

Wall boundary conditions were set to be smooth (no-slip condition), which means velocity at the wall has zero tangential components. The inflow boundary condition was set to be the velocity inlet type. The velocity profile is uniform, and its flowing direction was perpendicular to the inlet face. The air and water were mixed; then the mixture flowed along the main pipe. The main pipe was set to be long enough for the two-phase flow to be fully-developed before reaching the intersection. Here, the true air and water velocities were equal to air and water superficial velocities, respectively, due to only a single phase at the inlet. Table II shows eight testing combination of air and water velocities for parametric study.

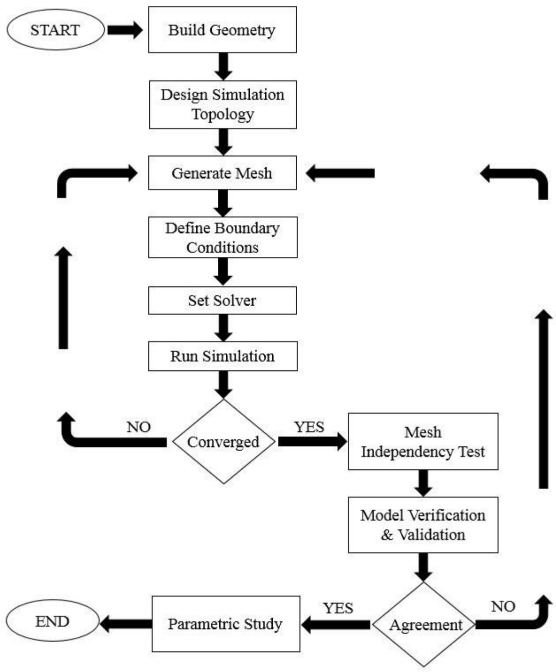

Fig. 3. Schematic of the modeling geometry domain of a converging T-junction.

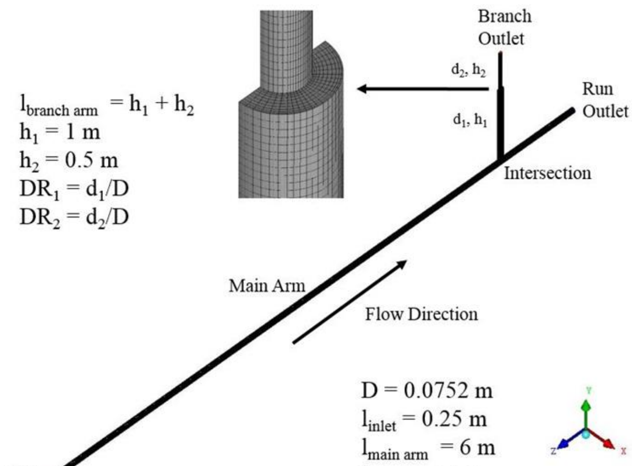

Fig. 4. Schematic of the modeling geometry domain of a converging T-junction.

With the properties of air and water assuming to be unchanged as shown in Table III, the mass flow rate of air and water can be calculated using Equation (1) and (2). Then, Equation (3) and (4) allows locating the testing point in Baker's map to validate slug flow.

TABLE I: TESTING GEOMETRY DESIGN NUMBER

Geometry Design Number (GDN)	DR_1	DR_2	Abbreviation
1	1.0	0.2	*DR* 1.0-0.2
2		0.5	*DR* 1.0-0.5
3		0.8	*DR* 1.0-0.8
4		1.0	*DR* 1.0-1.0
5	0.67	0.27	*DR* 0.67-0.27
6		0.4	*DR* 0.67-0.4
7		0.5	*DR* 0.67-0.5
8		0.67	*DR* 0.67-0.67

TABLE II: TESTING COMBINATION OF AIR & WATER VELOCITIES

Velocity Combination Number (VCN)	U_{SG} (m/s)	U_{SL} (m/s)
1	0.648	0.28
2	0.648	0.49
3	0.648	0.698
4	0.648	0.84
5	1.195	0.28
6	1.195	0.49
7	1.195	0.698
8	1.195	0.84

TABLE III: PROPERTIES OF TWO PHASES

	ρ (kg/m^3)	μ (Pa s)	σ (N/m)
Primary phase: air	998.6	0.08899	0.074
Secondary phase: water	1.225	0.001831	

$$G = \frac{\dot{m}_G}{A} = U_{SG}\rho_G \tag{1}$$

$$L = \frac{\dot{m}_L}{A} = U_{SL}\rho_L \tag{2}$$

$$\lambda = \left(\frac{\rho_G}{\rho_A}\frac{\rho_L}{\rho_W}\right)^{1/2} \tag{3}$$

$$\psi = \left(\frac{\sigma_W}{\sigma}\right)\left[\left(\frac{\mu_L}{\mu_W}\right)\left(\frac{\rho_W}{\rho_L}\right)^2\right]^{1/3} \tag{4}$$

At outflow boundary condition, no flow properties are specified, instead, normal gradients to the outflow plane of flow properties, for instance, velocity and turbulence quantities, were set to be zero ($dv/dz = 0$ at run outlet and $dv/dy = 0$ at branch outlet). Mass flow split was set to be 0.2, 0.4, 0.5, 0.6 and 0.8. The symmetry boundary condition enabled to model half of physical geometry domain, thus saving computational time. Mathematically, normal gradients to the symmetry plane of flow field variables were set to zero throughout the symmetry plane. Gravitational acceleration (g = 9.81 ms^{-2}) was applied in the reversed y-direction.

C. Solver Settings and Governing Equations

The VOF model using High-Resolution Interface Capturing (HRIC) scheme and the k-ε turbulence model with scalable wall function treatment was utilized to track and capture the slug flow in the T-junction. In the VOF modelling, the phases share a single set of conservation equations. A segregated pressure-based solver called Pressure Implicit with Split Operator (PISO) was chosen as the most appropriate method to solve governing equations. These governing equations can be written as:

- Mass conservation equation:

$$\frac{\partial}{\partial t}(\rho) + \nabla\cdot(\rho U) = 0 \tag{5}$$

- Momentum conservation equation:

$$\frac{\partial}{\partial t}(\rho U) + \nabla\cdot(\rho UU) = -\nabla p + \nabla\cdot\left[\mu\left(\nabla U + \nabla U^T\right)\right] + \rho g + F \tag{6}$$

- Turbulence equation:

$$\frac{\partial(\rho_m k)}{\partial t} + \nabla.(\rho_m k v_m) = \nabla.\left(\frac{\mu_{t,m}}{\sigma_k}\nabla k\right) + G_{k,m} - \rho_m\varepsilon \tag{7}$$

$$\frac{\partial(\rho_m \varepsilon)}{\partial t} + \nabla.(\rho_m \varepsilon v_m) = \nabla.\left(\frac{\mu_{t,m}}{\sigma_k}\nabla \varepsilon\right) + \frac{\varepsilon}{k}(C_{1\varepsilon}G_{k,m} - C_{2\varepsilon}\rho_m\varepsilon) \tag{8}$$

where t is time, U is the fluid velocity, p is the pressure, g is the gravitational acceleration, and F is the body forces.

D. Mesh Convergence Analysis

After generating a mesh with good quality, it is imperative to test if the solution is grid independent. The test purpose is to determine the mesh resolution which if it increases, the results should not change appreciably. In other words, it means the solution is not dependent on the mesh resolution. Otherwise, the result is meaningless if there is a significant difference between the two solutions from same-setting modelling. In three-dimensional flows, it is noted that if the one doubled the number of the interval in each direction, the number of cell increases by a factor of 8. Therefore, an increase in mesh resolution should be considered within the computing capacity.

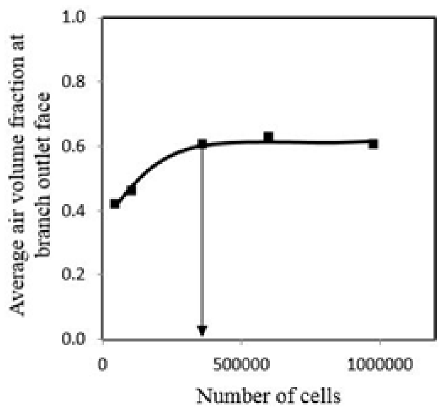

Fig. 5. Mesh independency test.

Regular T-junction was used for mesh independence test. Five cases with different mesh resolution were generated from very coarse to very fine mesh. Then all mesh cases were imported into the same-setting model. Average air fraction at the branch outlet plane was measured to determine the accuracy of the simulation. Fig. 5 presents that from medium case to the finer resolution, the observed parameters do not change appreciably. An increase of mesh resolution above medium case only wastes computing cost. A balanced approach to computing cost and solution accuracy should be compromised. Therefore, the medium grid of 357762 cells is adequately resolved, and its meshing density was chosen for all other geometry designs in this study.

E. Slug Flow Validation

For flow regime validation purpose with Baker's map, Table IV represents ten validation cases with different combinations of superficial air and water velocities taking from Saieed's and Zeeshan's experiment to generate slug flow [9], [16]. It is noted that the first three cases are for regular T-junction, the next three cases for reduced T-junction, and the last four cases for converging T-junction. These combinations of superficial velocities were within the slug region in Baker's map as shown in Fig. 6. This figure also presents the testing points for parametric design in Table II.

TABLE IV: TESTING COMBINATION OF AIR & WATER VELOCITIES

Cases	DR	U_{SG} (m/s)	U_{SL} (m/s)
1	1.0	1.4	0.21
2	1.0	1.4	0.28
3	1.0	1.4	0.49
4	0.67	1.4	0.21
5	0.67	1.4	0.28
6	0.67	1.4	0.49
7	1.0 - 0.5	0.648	0.28
8	1.0 - 0.2	0.648	0.28
9	0.67 - 0.5	0.648	0.28
10	0.67 - 0.27	0.648	0.28

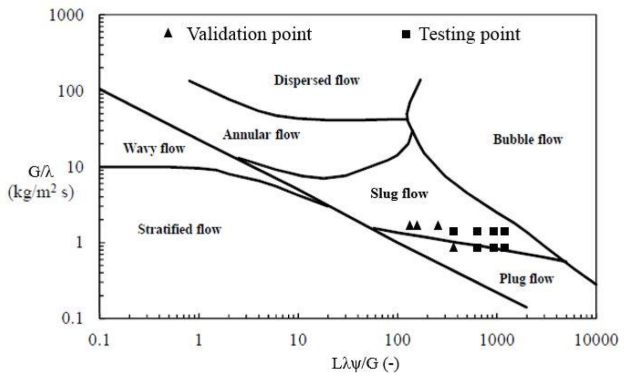

Fig. 6. Validation and testing points in Baker's map.

The elongated gas slugs were detected at the top of the pipe, between the liquid slugs as shown in Fig. 7. This figure also presented the cross-sectional contours of the water volume fraction at seven different locations for the present slug flow model. At 75D position, an elongated bubble was generated at the upper part of the pipe. Moving along the pipe, the volume fraction of air reduced until the liquid slug completely blocked the pipe at 80D. Next, a smaller elongated gas slug together with small gas bubbles was shown at 84D, followed by another liquid slug and third gas slug at the end. These slugs moved along the pipe until it reached the T-junction.

As discussed in the literature, the local pressure built up in the liquid slug drove the mechanism of slug flow generation continuously. To validate the present model with this theory, Fig. 8 described the pressure distribution on the symmetry plane. It is clear that the pressure in the front of the slug was very high compared with that at the slug tail due to the slug blockage. This pressure force drove the slug moving along the pipe.

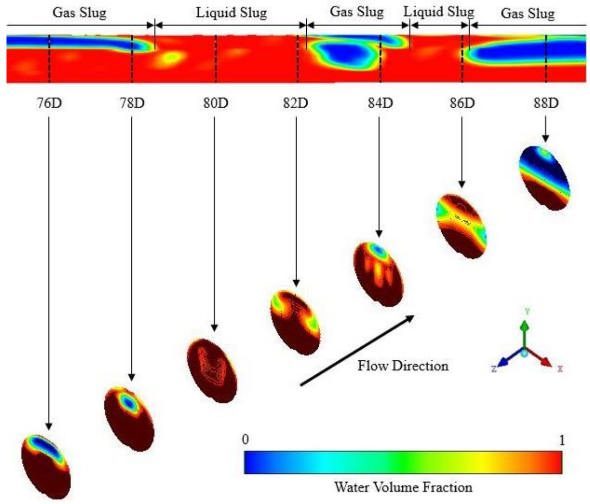

Fig. 7. Cross-sectional contour for slug flow regime.

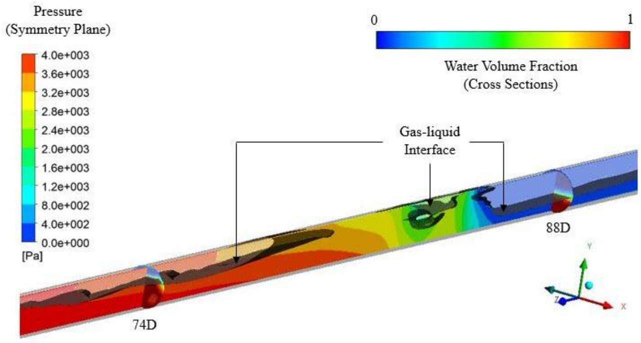

Fig. 8. Pressure distribution on the symmetry plane and gas-liquid interface of the slug flow in the main arm.

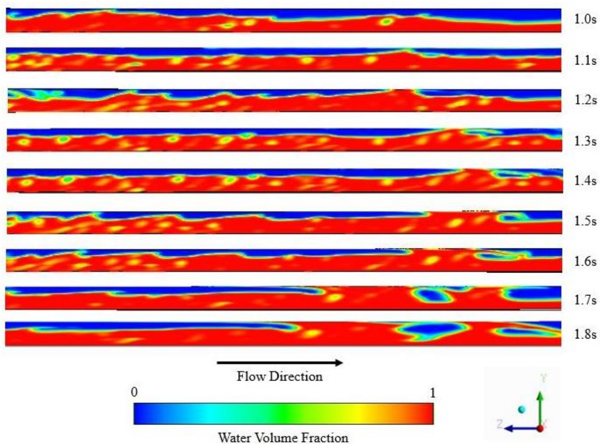

Fig. 9. Contour of slug flow transition in the main arm from 1.0s to 1.8s.

For slug flow transition validation, Fig. 9 shows contours of water volume fraction at the different time frame from 1.0s to 1.8s, in order to illustrate the slug initiation process. The red and blue color represent pure liquid and gas respectively. At 1.0s, the flow regime was observed as stratified-wavy. Some very first small gas bubbles appeared in the liquid, later their number increased dramatically. At 1.2s, the liquid started to reach the top of the pipe, then higher pressure was built up at the front until the complete cross-section was blocked at 1.5s. Then, more liquid was accumulated at the slug, and the gathering gas bubbles formed the elongated gas slug which moved along with the liquid.

From above slug flow validation, it can be concluded that the present model was able to generate slug flow and illustrate the unsteadiness of slug behavior at the main arm. This very good result was due to the VOF enhancing tracking precise interface between air and water together with sinusoidal perturbation initialization.

F. Phase Separation Validation

To validate phase separation with experiment data, the ratio of the mass flow rate at branch arm and main arm, namely fraction of air (F_a) and water (F_w) going to branch arm, is used as indicators of phase distribution as described in equation (9), (10). Meanwhile, mass flow rate ratio is expressed as equation (11).

$$F_a = \frac{m_{a3}}{m_{a1}} \tag{9}$$

$$F_w = \frac{m_{w3}}{m_{w1}} \tag{10}$$

$$F = \frac{m_3}{m_1} \tag{11}$$

where 1, 2, 3 are the subscripts of main, run and branch arms, *w*, *a* are the subscripts of water and air.

The standard error of the estimate (SEE) calculated as Equation (12) was used to determine the error of predicted simulation results compared to experiment. Here, y is the experiment data, y_{est} is the simulation results, n is number of given data.

$$SEE = \sqrt{\sum \frac{(y - y_{est})^2}{n}} \tag{12}$$

The volume fraction of air and water at the branch was chosen to represent the phase separation data. Simulation data were linearly interpolated to calculate error with experimental data points. The averaged SEE relative to Saieed's [12] data is 7.58 %, respectively, which are acceptable for the flow split prediction. Therefore, regular and reduced T-junction models can be used for further investigation.

To validate the phase split in converging T-junction, the experimental data from Zeeshan was chosen. Table IV presents four validation cases from 7 to 10 for converging T-junctions with the same superficial velocities of air and water, U_{SG} = 0.648 m/s, U_{SL} = 0.28 m/s. Using the same previous method of evaluating the error between simulation and experimental data. Here, the averaged SEE relative to experimental data was 6.26%. It can be concluded that the converging model was good for further investigation.

G. Separation Efficiency

Dimensionless area, *S*, under the curve of phase separation is proposed to use as a single-valued scalar indicator to evaluate a T-junction's performance. *S* is a dimensionless parameter defined as the area of the region bounded by the axis and linear interpolated curve from a set of data of air and water fraction. As shown in Fig. 10, the representation of fraction of air and water can be divided into three areas: the upper triangle, the lower triangle and the equal split line, thus S can be expressed as Equation (13) corresponding to these areas. The lower triangle area indicates the air-dominated flow in the branch arm. In case of the upper triangle area, it presents the water-dominated flow in the branch arm and the air-dominated flow in the run arm. Here, the role of run and branch arm can be interchanged. At the equal split line, the air fraction is equal to the water fraction, which is the worst case of separation. Due to limited set of data, the area under the curve can be calculated using standard numerical integration formula, e.g., trapezoidal rule. From common sense, optimum T-junction should have a minimum *S*.

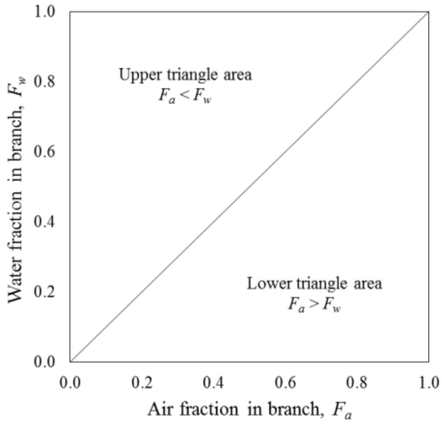

Fig. 10. Representation of volume fraction of air and water, divided into three areas.

$$S = \begin{cases} \int_0^1 F_w dF_a & : \; F_a > F_w \\ 0.5 & : \; F_a = F_w \\ \int_0^1 F_a dF_w & : \; F_a < F_w \end{cases} \tag{13}$$

Based on the area under the curve of phase separation (*S*), a new criterion, separation efficiency (*SE*), is proposed as Equation (14). Here, S_{max} is the maximum area under the curve of phase separation. From Equation (13), S_{max} is equal to 0.5, in which the separation efficiency is as low as 0 %. Meanwhile, the corners of Fig. 10, (0,1) or (1,0) are conditions of complete separation. The closer of the separation curve to these points, the higher separation efficiency is.

$$SE = \frac{S_{max} - S}{S_{max}} \times 100\% \tag{14}$$

III. Results and Discussion

A. Phase Separation Behavior

After generating successfully the slug flow at the main arm as discussed in the validation section, the phase separation behavior at the intersection of the T-junction was investigated. Fig. 11 illustrates the contour of pressure distribution on the symmetry plane and the gas-liquid interface of the slug flow reaching the intersection of the T-junction. This was recorded at 1.2s for the GDN 2 with VCN 1.

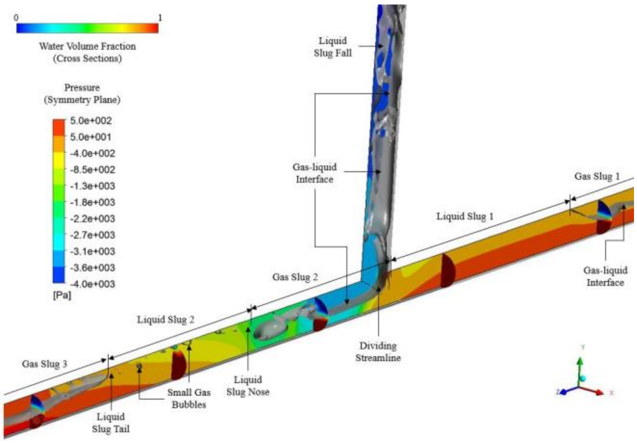

Fig. 11. Pressure distribution on the symmetry plane and gas-liquid interface of the slug flow reaching the intersection of T-junction at 1.22s

When the liquid slug 1 passed the intersection, a part of liquid was extracted into the branch arm. This was because of very high pressure drop between the main pipe and the branch arm as shown in pressure contour. The liquid carryover was likely to "climb" the wall of branch arm to form a slug jump, then its momentum decreased on the way due to gravitational forces and friction loss. Thus, a portion of slug dropped back into the main inlet as the slug fall. On the way, it encountered the very high-speed airflow, which made the behavior of slug fall more complicated. Meanwhile, most of the gas slug 2 continuously entered the branch arm because the liquid slug 1 blocked the run arm. A "dividing streamline" as mentioned by Liu and Li [17], was formed clearly at the intersection. This allowed the gas to divert faster into the branch arm and dominate the space at the entrance of branch arm. Hence, the pressure difference between two areas separated by the streamline was very high. Here, the gas- dominated area above the streamline was in blue color, while liquid-dominated area under the streamline was in orange or red color. Because of less gas going to the run arm, the pressure distribution in liquid slug 1 at the run arm was quite homogeneous. In contrast, the pressure distribution in liquid slug 2 varied significantly along the moving direction. This was caused by an amount of gas entrained into the liquid slug in the form of small gas bubbles at the top of the pipe. The pressure at the slug tail was much higher than it at the slug nose, which generated the kinetic energy for the liquid slug to move along the main pipe.

The cross-sections at different locations also showed the change of slug flow in the main pipe. At the gas slug 3, the volume fraction of gas and liquid was 50:50. However, in the liquid slug 2, only a small volume fraction of gas appeared at the top as the gas bubbles. Then, these small bubbles were gathered and bigger bubbles were formed. These bubbles were likely to be attracted to the gas slug 2, then going to the branch arm. Hence, the cross-section at the liquid slug 1 was full of liquid. A new cycle was repeated for the next liquid slug.

In Fig. 12, once the nose of liquid slug 2 reached the intersection at 1.29s, most of the gas slug 2 was diverted into the branch arm. As a result, more liquid was dragged into the branch arm and more slug jump was generated. Thus, the pressure at branch arm and liquid slug 2, as well as gas slug 3, reduced remarkably. Meanwhile, the pressure at the liquid slug 1 and gas slug 1 in the run arm still remained unchanged. Here, the dividing streamline kept its important role in diverting the gas flow from gas slug 2. It is noted that at this stage when the gas slug was extracted and the nose of the liquid slug reached the intersection, the liquid carryover was highest.

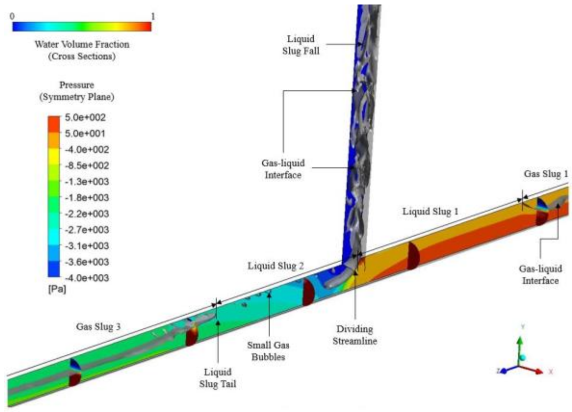

Fig. 12. Pressure distribution on the symmetry plane and gas-liquid interface of the slug flow reaching the intersection of T-junction at 1.29s.

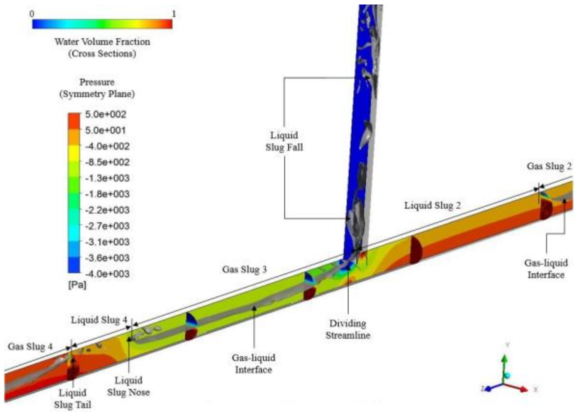

Fig. 13. Pressure distribution on the symmetry plane and gas-liquid interface of the slug flow reaching the intersection of T-junction at 1.42s.

In Fig. 13, when the liquid slug 2 and gas slug 2 passed through the intersection and entered the run arm at 1.42s, the gas slug 3 started to reach the intersection. At this point, less liquid was dragged into the branch arm, more liquid fell back into the main pipe due to a lack of momentum dragged force. The pressure built up in liquid slug 4 and gas slug 4 was the same as liquid slug 2 and gas slug 3 as illustrated in Fig. 11. It is noted that in this stage, the liquid carryover was lowest. When the liquid slug 4 reached the intersection, the behavior of slug flow was repeated as described in Fig. 11.

B. Effect of Converging Diameter Ratio

Fig. 14 presented the relationship between the separation efficiency (SE) and converging diameter ratio (DR_2). In the GDN 1-4 with main diameter ratio (DR_1) of 1.0, the regular

T-junction delivered the lowest separation efficiency, which means the highest amount of liquid carryover. When the converging diameter ratio decreased from 1.0 to around 0.5, the separation efficiency increased gradually at all combinations of GDN and VCN. Compared with regular T-junction, the converging design can improve up to 20% of separation efficiency in case of converging diameter ratio of 0.5. However, a further drop of converging diameter ratio to 0.2, did not improve the phase separation such as VCN 4 and 8. The separation efficiency even showed a slight decrease, for example, at VCN 5. Theoretically, two principles drive this phenomenon. Firstly, while the main diameter ratio was kept unchanged, a reduction of converging diameter ratio caused the liquid carryover rising near the wall to be blocked and then dropped back into the main pipe. The high-speed air entering the branch arm dragged liquid in the annular patterns, which means the air was moving in the core and the liquid was moving in the near-wall region. This effect reduced the liquid carryover going to the converging pipe section. Secondly, a smaller conduit in the converging pipe section also reduced space for the liquid to be dragged by the airflow. However, when the converging diameter ratio became as small as 0.2, smaller conduit accelerated the airflow due to the Bernoulli's principle. This caused a very high pressure drop between the branch outlet and the inlet of the converging pipe section, which slightly increased the liquid carryover as observed in Fig. 14.

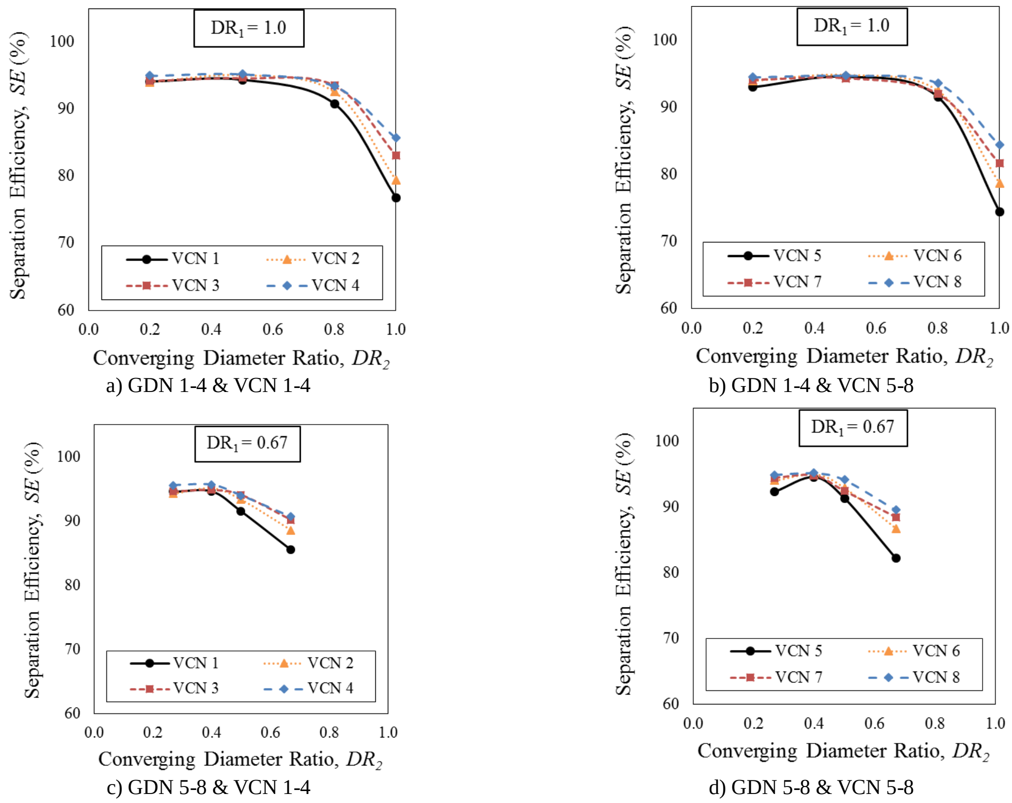

Fig. 14. Effect of converging diameter ratio (DR_2) on separation efficiency (SE).

In case of GDN 5-8 with main diameter ratio (DR_1) of 0.67, in spite of higher increasing rate of separation efficiency compared with GDN 1-4 when the converging diameter ratio decreased, the overall trend was similar to the previous discussion. Here, the optimal design with a converging diameter ratio of 0.4 can improve by up to 12% of separation efficiency compared with reduced T-junction. Therefore, it can be concluded that the converging T-junction yielded better performance in phase separation compared with regular and reduced T-junction. Moreover, GDN 6 was observed as the optimal design to generate highest separation efficiency of 95.65%.

C. *Effect of Phase Superficial Velocity*

Fig. 15 presents the relationship between separation efficiency (SE) and the water superficial velocity (U_{SL}). In general, the result showed an excellent agreement with the theoretical understanding that an increase in water superficial velocity will decrease the liquid carryover. The trend was evident for all combinations of GDN and VCN. It was also noticeable that the effect of water superficial velocity was strong in regular and reduced T-junctions as GDN 4 and 8, respectively, while converging T-junctions showed a weaker influence in reducing liquid carryover when increasing water superficial velocity.

In order to evaluate the effect of air superficial velocity on phase separation efficiency (SE), it is essential to compare among combinations having the same GDN and water superficial velocity. Fig. 16 presented the separation efficiency (SE) versus the air superficial velocity (U_{SG}), which were divided into four groups. It can be seen that when the air superficial velocity increased, separation efficiency decreased slightly, which means more liquid carryover at the branch arm. The explanation to this phenomenon is, with the increase in air superficial velocity, the higher centripetal force at the intersection caused an increase in pressure drop between the main arm and branch arm. Then, this pressure drop forced the liquid to be sucked into the branch arm. This result agreed with previous work such as Hong [1]. From Fig. 16, it was also noticed that this effect was robust in case of GDN 4 and 8 (regular and reduced T-junctions) and weak in case of converging T-junctions.

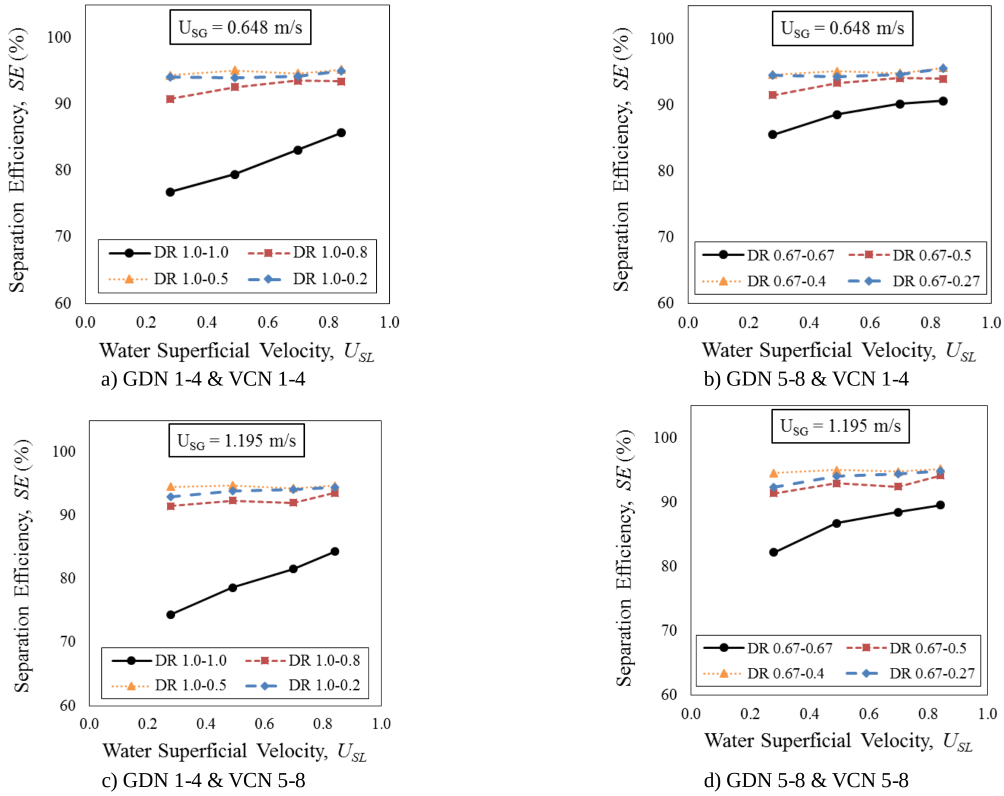

Fig. 15. Effect of water superficial velocity (U_{SL}) on separation efficiency (SE).

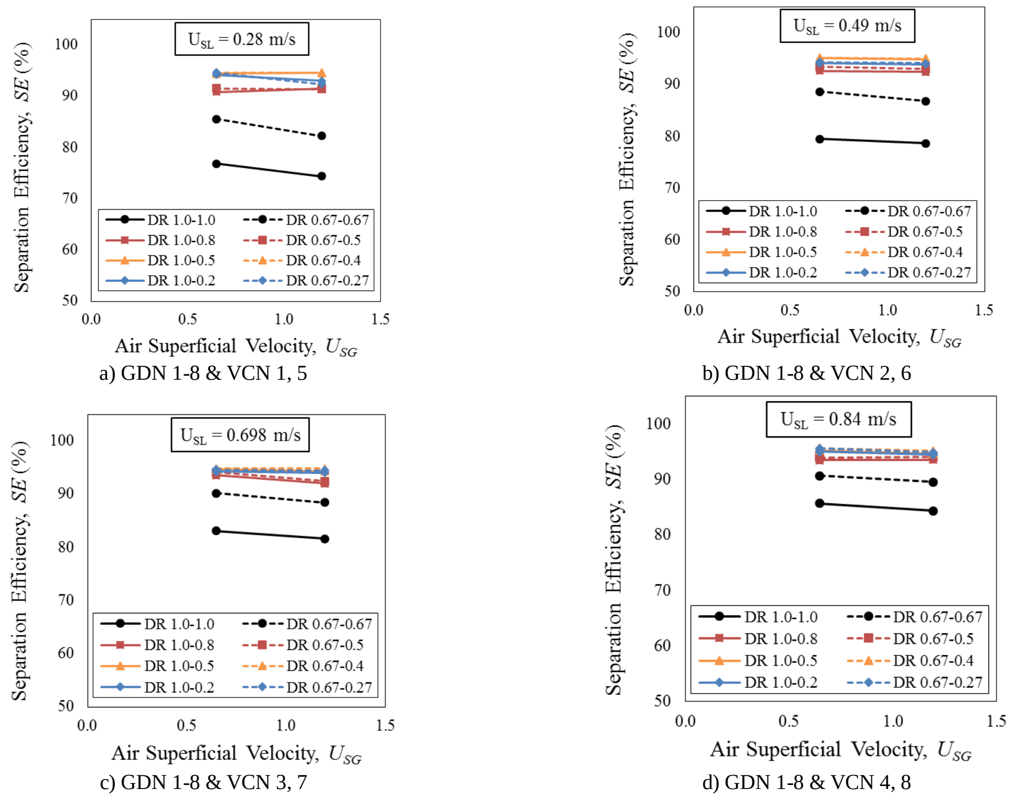

Fig. 16. Effect of air superficial velocity (U_{SG}) on separation efficiency (SE).

Overall, the air and water superficial velocities had a massive influence on the amount of liquid extracted into the branch arm in regular, reduced and converging T-junctions. While an increase in water superficial velocity improved the phase separation efficiency, an increase in air superficial velocity worsen the liquid carryover phenomenon. Specifically, the level of these effects was found to be dependent on the geometry design, which means the main and converging diameter ratios. In addition, the water superficial velocity was found to generate more influence on separation efficiency than air superficial velocity over the investigated range.

D. Correlations

From the above analysis, separation efficiency (SE) was a reliable tool to evaluate the phase separation of a T-junction. This work focused on investigating the direct factors affecting separation efficiency, through which can determine the optimal performance. These factors included the superficial velocities of air and water, the main diameter ratio and the converging diameter ratio.

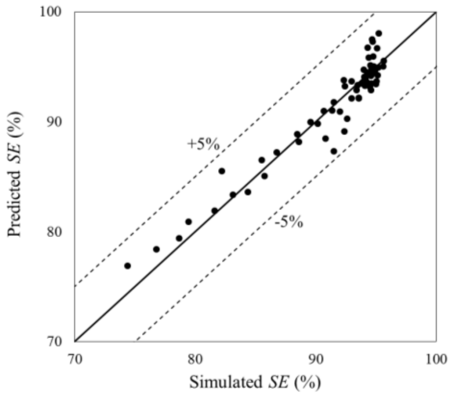

Fig. 17. Comparison of simulated and predicted values of the area under the curve of phase separation efficiency (S).

From the design of parametric study, a data set of 64 points was used to build a correlation of the separation efficiency (SE) regarding those factors mentioned above. Equation (15) presented the correlation developed for predicting separation efficiency as followed. The predicted value obtained from Equation (15) were compared with simulation data, which resulted in a plot as shown in Fig. 17. This figure suggested that 100% of the predictions are in the span of 5% error.

$$\begin{aligned} SE = 95.02 - 6.328DR_1 + 16.02U_{SL}DR_2 - 4.108U_{SL}DR_1 \\ - 2.669U_{SG}DR_2 + 39.71DR_1DR_2 - 51.62DR_2^2 \end{aligned} \tag{15}$$

IV. Conclusion

The research reported numerical analysis of phase separation behavior of air-water two-phase slug flow in eight different designs of T-junction including regular, reduced and converging T-junction. These designs have a horizontal main pipe with diameter of 0.0752 m and vertical branch arm with diameter value characterized by main and converging diameter ratios. Based on the results, conclusions could be drawn:

- The plot of volume fraction of air versus water at the branch arm was very useful to have an overview of phase separation performance of T-junction. However, the liquid carryover threshold and the peak liquid carryover were not sufficient to evaluate and compare phase split among different operating conditions and T-junction's designs.
- The separation efficiency (SE) was proved as a reliable tool to evaluate the phase separation performance. It was observed that for the best phase separation, a T-junction must have a high separation efficiency.
- In all regular, reduced and converging T-junctions, the separation efficiency adopted an increasing trend when the liquid superficial velocity increased. Meanwhile, it was in an inverse relationship with gas superficial velocity.
- It was also discovered that overall, the separation efficiency was in an inverse relationship with the main diameter ratio. Meanwhile, it was likely to increase when the converging diameter ratio decrease to a certain limit. Then a further drop of converging diameter ratio from that limit slightly decreased the separation efficiency.
- Among 8 designs of T-junction, it was found that the converging T-junctions can improve by up to 20% and 12% compared with regular and reduced T-junctions, respectively. This discovery proved the hypothesis of this study. The optimal combination of main and converging diameter ratios was DR 1.0-0.5 and DR 0.67-0.4. Here, the latter design showed slightly better performance with 95.65% of separation efficiency.
- In future works, the optimized T should be tested in wider range of velocities as well as flow regimes.

Nomenclature

A	cross-sectional area	m^2
C_D	drag force coefficient	
d	pipe diameter	m
f	drag force	Nm^{-3}
F	mass flow rate ratio	
g	gravitational acceleration	ms^{-2}
G	gas mass flux	$kgm^{-2}s^{-1}$
G_k	generation of turbulent kinetic energy	
I	unit tensor	
k	turbulent kinetic energy	m^2s^{-2}
L	liquid mass flux	$kgm^{-2}s^{-1}$
LCT	liquid carryover threshold	
m	mass flow rate	kgs^{-1}
P	mixture pressure of 2 phases	Pa
PLC	peak liquid carryover	
R	body force (between 2 phases)	N
R_e	relative Reynolds number	
S	area of liquid carryover	
SEE	standard error of the estimate	
U	Velocity	ms^{-1}
U_S	Superficial Velocity	ms^{-1}

Greek letters

α	volume fraction	
ε	turbulent dissipation rate	m^2s^{-3}
μ	dynamic viscosity	$kgm^{-2}s^{-1}$
μ_t	turbulent viscosity	$kgm^{-2}s^{-1}$
σ	surface tension coefficient	Nm^{-1}
ρ	density	kgm^{-3}
τ	stress strain tensor	
υ	kinematic viscosity	m^2s^{-1}

Subscripts

1,2,3	main, run, branch arms
a	air
g	gas phase
i	g or l
l	liquid phase
m	two-phase mixture
w	water

Conflict of Interest

The authors declare no conflict of interest.

AUTHOR CONTRIBUTIONS

Minh Cong Tran, Hai Anh Nguyen conducted the research and analyzed the data. Dat Tien Nguyen wroted the paper. All authors had approved the final version.

ACKNOWLEDGMENT

This research was supported by Viettel High Technologies Corporation, Viettel Group in the research program of Modeling & Simulation Center and Control & Dynamic Department.

REFERENCES

[1] K. C. Hong, "Two-phase flow splitting at a pipe tee," *Journal of Petroleum Technology*, vol. 30, pp. 290–296, 1978.

[2] Y. Taitel and D. Barnea, "Two-phase slug flow," in *Advances in Heat Transfer*, J. P. Hartnett and T. F. Irvine, Eds. Elsevier, 1990, vol. 20, pp. 83–132.

[3] A. R. Kabiri-Samani and S. M. Borghei, "Pressure loss in a horizontal two-phase slug flow," *J. Fluids Eng*, vol. 132, 2010.

[4] E. Wren, "Geometric effects in phase split at a large diameter T-junction," doctoral thesis, University of Nottingham: UK, 2001.

[5] B. J. Azzopardi, "The effect of side arm diameter on phase split at t-junctions," in *Proc. the SPE Annual Technical Conference and Exhibition*, Houston, Texas, USA, 1999.

[6] S. Griston and J. H. Choi, "Two-phase flow splitting at side-branching tees," in *Proc. the SPE Western Regional Meeting*, Society of Petroleum Engineers, 1998.

[7] J. Reimann, H. J. Brinkmann, and R. Domanski, "Gas-liquid flow in dividing T-junctions with a horizontal inlet and different branch orientations and diameters," KfK4399, Technical University of Warsaw: Poland, 1988.

[8] F. Peng and M. Shoukri, "Modelling of phase redistribution of horizontal annular flow divided in T-junctions," *The Canadian Journal of Chemical Engineering*, vol. 75, pp. 264–271, 1997.

[9] A. Saieed, "Experimental investigation on the effect of the diameter ratio on two-phase separation in a T-junction," MSc thesis, Universiti Teknologi PETRONAS: Malaysia, 2017.

[10] M. Cook and M. Behnia, "Bubble motion during inclined intermittent flow," *International Journal of Heat and Fluid Flow*, vol. 22, pp. 543–551, 2001.

[11] D. Lorstad and L. Fuchs, "High-order surface tension VOF-model for 3D bubble flow with high-density ratio," *Journal of Computational Physics*, vol. 200, pp. 153–176, 2004.

[12] L. Zhou, D. Liu, and C. Ou, "Simulation of flow transients in a water filling pipe containing entrapped air pocket with vof model," *Engineering Applications of Computational Fluid Mechanics*, vol. 5, pp. 127–140, 2011.

[13] T. Taha and Z. F. Cui, "CFD modelling of slug flow in vertical tubes," *Chemical Engineering Science*, vol. 61, pp. 676–687, 2006.

[14] P. M. Ujang, C. J. Lawrence, C. P. Hale, and G. F. Hewitt, "Slug initiation and evolution in two-phase horizontal flow," *International Journal of Multiphase Flow*, vol. 32, pp. 527–552, 2006.

[15] M. Febres, A. O. Nieckele, and R. Fonseca, "Three-dimensional unit slug in a horizontal pipeline," in *Proc. the 7th International Conference on Multiphase Flow*, Florida USA, 2010.

[16] M. Zeeshan, "Experimental investigation on two-phase separation in a converging T-junction," MSc Thesis, Universiti Teknologi PETRONAS: Malaysia, 2019.

[17] Y. Liu and W. Z. Li, "Numerical simulation on two-phase bubbly flow split in a branching T-junction," *Int. J. Air-Cond. Ref.*, vol. 19, pp. 253–262, 2011.

Minh Cong Tran is currently a modeling & simulation engineer at Modeling & Simulation Center, Viettel High Technology Industries Corporation. His background and research interest includes dynamics modeling & control system and numerical simulation.

Hai Anh Nguyen is currently a modeling & simulation engineer at Modeling & Simulation Center, Viettel High Technology Industries Corporation. His background and research interest includes dynamics modeling & control system and numerical simulation.

Dat Tien Nguyen is currently a modeling & simulation engineer at Modeling & Simulation Center, Viettel High Technology Industries Corporation. His background and research interest includes dynamics modeling & control system and numerical simulation.

Hai Anh Nguyen holds a bachelor in aerospace engineering from the excellent engineers training program in Hanoi University of Science and Technology (HUST) and master in aerospace engineering in Institute Teknologi Bandung (ITB), Bandung, Indonesia.